Computer simulation of the structure and elasticity of polyurethane networks: 2. Polyoxypropylene triols and 4,4′-diphenylmethane diisocyanate

K.-J. Lee and B. E. Eichinger*
Department of Chemistry, BG-10, University of Washington, Seattle, WA 98195, USA
(Received 24 March 1989; revised 23 June 1989; accepted 8 July 1989)

Polyoxypropylene triol-based urethane networks have been simulated with a computer. Simulations show that cyclic molecules are present in substantial amounts in the sol fraction when the stoichiometric ratio $r_s \sim 1.0$. Simulations also show that the fractions of loops are much higher than those obtained from modified cascade theory. The population of loops is dependent on molecular weight, dilution and stoichiometric ratio. The proportion of dangling ends is independent of molecular weight and dilution, but depends upon r_s. It is found that, for $r_s \sim 0.8$–1.0, the simulations underestimate moduli, but they give very good agreement either for the affine model or for the phantom model when r_s is below 0.8. Reasons for the discrepancy are given in terms of segmentation effects known to occur with the 4,4′-diphenylmethane diisocyanate used in the experimental work.

(Keywords: urethane; networks; polyoxypropylene; elasticity)

INTRODUCTION

The algorithm used in the preceding paper[1] (referred to as paper 1) is used here to simulate polyoxypropylene (POP) and diisocyanate by some appropriate modifications. Once again, the configurations of POP triols are generated by a Monte Carlo method[2–7] that is described by the rotational isomeric state (RIS) theory[8]. Ilavský and Dušek[9–11] have studied the structures and physical properties of model networks prepared from polyols and diisocyanates to test the validity of elasticity theories.

The systems that are investigated in this paper were studied experimentally by Ilavský and Dušek[9,10]. In their studies, one series of networks was prepared from Union Carbide Niax polyols (LG-56 and LHT-240, whose chemical structures are shown in *Figure 1*) and 4,4′-diphenylmethane diisocyanate (MDI) in the bulk at 55–60°C[9]. Another series of samples was prepared in various solutions by polymerization of LHT-240 with MDI at room temperature and then at 70°C[10]. The equilibrium moduli were measured at 60°C for the samples prepared in the bulk[9] and at 25°C for those cured in solution[10].

In the cited work, the concentration of elastically active network chains was derived from Dušek's modified branching theory[12]. The extent of reaction of NCO groups was calculated from the weight fraction of the sol by use of the same theory. The fraction of bonds wasted in elastically inactive cycles was determined from the probability that the end-to-end vectors of Gaussian chains are equal to zero[12,13]. The purpose of this paper is to compare computer-generated network structures with the results of measurements and with the predictions of branching theory.

STATISTICAL WEIGHT MATRICES FOR POP TRIOLS

Figure 1 represents the chemical formulae of Niax triols LHT-240 and LG-56; the numbers 1, 2 and 3 label the three arms of the triols. In order to calculate the distances between two –OH groups on the same molecule by use of the RIS scheme, the centre carbon (*C) in *Figure 1* is assumed to adopt three conformations (*Figures 2* and *3*). The statistical weight matrices of equations (1) in paper 1 are applied to the repeating units in the parentheses in *Figure 1*. The values of the bond lengths, supplements of the bond angles, and the conformation energies are the same as those used there. The statistical weight matrices for the rest of the bonds that are not repeating were obtained by the procedure of Abe *et al.*[14] for POP carrying side-groups. The details of the derivation are described below.

Niax triol LG-56

The three conformations dependent on carbon (*C) are represented by *Figure 2*. The statistical weight matrices for *Figure 2a* are taken from POE (polyoxy-

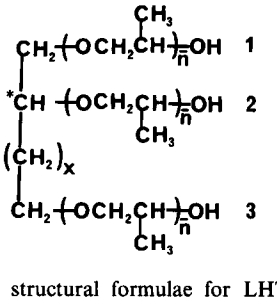

Figure 1 Chemical structural formulae for LHT-240 and LG-56: LHT-240, $x=3$, $\bar{n} \simeq 4$; LG-56, $x=0$, $\bar{n} \simeq 15$

* To whom correspondence should be addressed

0032-3861/90/030414-09
© 1990 Butterworth & Co. (Publishers) Ltd.

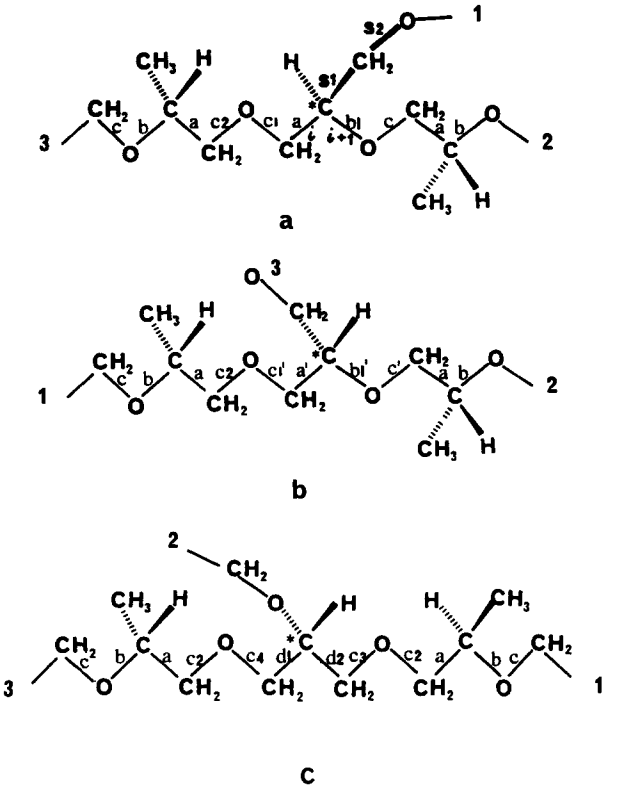

Figure 2 Three conformations for LG-56 to calculate end-to-end distances between two –OH groups. (a) Arm 1 is treated as side-chain. (b) Arm 3 is treated as side-chain. (c) Arm 2 is treated as side-chain

ethylene) and POM_3 (polyoxytrimethylene) in the work of Abe and Mark[15] and from POP (paper 1). Hereafter, the statistical weight parameters with numerical subscripts are the same as those of the polyoxide series in ref. 15. The statistical weight matrix for bond b1 (*Figure 2a*) may be obtained by following the procedure of Abe *et al.*[14]. The first- and second-order interactions that are influenced by rotating the articulated bond s1 can be evaluated for each of the fixed rotational states about skeletal bonds i and $i+1$ (*Figure 2a*) on both sides of the carbon (*C). The results of the first- and second-order interactions are derived in a matrix form:

$$V=\begin{bmatrix} \omega_3+\alpha\omega_2+\beta & \omega_3+\alpha+\beta\omega_2 & \omega_3+\alpha+\beta \\ 1+\alpha\omega_2+\beta & 1+\alpha+\beta\omega_2 & 1+\alpha+\beta \\ 1+\alpha\omega_2+\beta\omega_3 & 1+\alpha+\beta\omega_2\omega_3 & 1+\alpha+\beta\omega_3 \end{bmatrix} \quad (1)$$

where α and β are the statistical weight parameters assigned to the first-order interactions for bond s1 in the g^+ and g^- states, respectively. Statistical weight parameters[15] ω_2 and ω_3 denote the second-order interactions. Energies, E_α and E_β, corresponding to statistical weight parameters α and β, are the same conformational energies associated with the rotation about bond a of POP (*Figure 2* in paper 1). The energies corresponding to ω_2 and ω_3 have been assigned[15] the values 0.4 and 0.6 kcal mol^{-1}, respectively. When each element $u_{\xi\eta}$ of the matrix U_b^R given in equation (1b) of paper 1 is multiplied by the corresponding statistical weight factor $V(\xi\eta)$, one may obtain the statistical weight matrix:

$$U_{b1}=\begin{bmatrix} \omega_3+\alpha\omega_2+\beta & 0 & \omega_3+\alpha+\beta \\ 1+\alpha\omega_2+\beta & 0 & \omega(1+\alpha+\beta) \\ 1+\alpha\omega_2+\beta\omega_3 & 0 & 1+\alpha+\beta\omega_3 \end{bmatrix} \quad (2)$$

for bond b1. Inspection of a model shows that the statistical weight matrices for bonds c1 and c2 (see *Figure 2a*) are:

$$U_{c1}=\begin{bmatrix} 1 & 0 & \sigma'_2 \\ 1 & \sigma'_2 & \sigma'_2\omega_2 \\ 1 & \sigma'_2\omega_2 & 0 \end{bmatrix} \quad (3)$$

and

$$U_{c2}=\begin{bmatrix} 1 & \sigma'_2 & \sigma'_2 \\ 1 & \sigma'_2 & 0 \\ 1 & 0 & \sigma'_2 \end{bmatrix} \quad (4)$$

respectively. Here the energies corresponding to σ'_2 and ω_2 are 0.9 and 0.4 kcal mol^{-1} (ref. 15), respectively. The rest of the statistical weight matrices for bonds a, b and c in *Figure 2a* are the same as those of POP described by equations (1) of paper 1.

The statistical weight matrices for bonds a', b1', c' and c1' in *Figure 2b* are obtained by treating respectively, U_a^R U_{b1}, U_c^R and U_{c1} with equation (2) in paper 1, with U_a^R and U_c^R given there in equations (1a) and (1c). The matrix for bond c2 is the same as equation (4).

If the procedure described above to obtain the statistical weight matrices for *Figure 2a* is followed, the matrices for bonds d1, d2, c3 and c4 (see *Figure 2c*) can be formulated respectively as:

$$U_{d1}=\begin{bmatrix} 1 & \beta & \sigma_3 \\ 1 & \beta\omega_2 & 0 \\ \omega_2 & 0 & \sigma_3\omega_2 \end{bmatrix} \quad (5)$$

$$U_{d2}=\begin{bmatrix} \omega_2\sigma_2(1+\sigma'_2) & \sigma_3(\omega_2+\sigma'_2) & \beta(\omega_2+\sigma'_2) \\ \sigma_2(1+\sigma'_2\omega_2) & \sigma_3(1+\sigma'_2) & \beta\omega_3(1+\sigma'_2) \\ \sigma_2(1+\sigma'_2\omega_2) & \sigma_3\omega_3(1+\sigma'_2) & \beta(1+\sigma'_2) \end{bmatrix} \quad (6)$$

$$U_{c3}=\begin{bmatrix} 1 & \sigma'_3\omega_2 & \sigma'_3 \\ 1 & \sigma'_3 & 0 \\ 1 & 0 & \sigma'_3\omega_2 \end{bmatrix} \quad (7)$$

and

$$U_{c4}=QU_{c3}Q \quad (8)$$

where the energies corresponding to statistical weight matrices ω_3, σ_3 and σ'_3 have been assigned the values 0.6, −0.4 and 0.9 kcal mol^{-1} in POM_3 (ref. 15), respectively. Here Q has been given in equation (3) of paper 1.

Niax triol LHT-240

The chemical structure of LHT-240 is similar to that of LG-56, except for $x=3$ (*Figure 1*). Thus, the procedure used to obtain the statistical weight matrices for LG-56 is applicable here to LHT-240. The three conformations based on centre carbon (*C) are summarized in *Figure 3*. In the following matrices, only those that differ from those of LG-56 are written.

The statistical weight parameters for bonds e1, e2, e3 and c11 in *Figure 3a* are taken from PM (polymethylene) and POM_4 (ref. 15). With the aid of a model, U_{e1}, U_{e3} and U_{c11} are given respectively as:

$$U_{e1}=\begin{bmatrix} 1 & 0 & \sigma'_4 \\ 1 & \sigma'_4 & \sigma'_4\omega_4 \\ 1 & \sigma'_4\omega_4 & 0 \end{bmatrix} \quad (9)$$

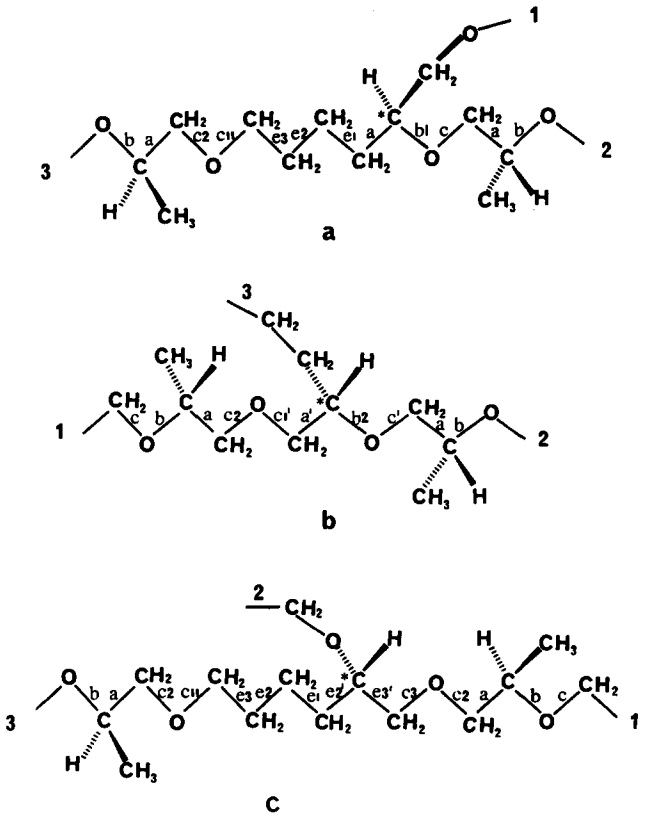

Figure 3 Three conformations for LHT-240 to calculate end-to-end distances between two –OH groups. (a) Arm 1 is treated as side-chain. (b) Arm 3 is treated as side-chain. (c) Arm 2 is treated as side-chain

$$U_{e3}=\begin{bmatrix}1 & \sigma_4 & \sigma_4\\ 1 & \sigma_4 & \sigma_4\omega_4\\ 1 & \sigma_4\omega_4 & \sigma_4\end{bmatrix} \tag{10}$$

and

$$U_{c11}=\begin{bmatrix}1 & \sigma_4'' & \sigma_4''\\ 1 & \sigma_4'' & 0\\ 1 & 0 & \sigma_4''\end{bmatrix} \tag{11}$$

where energies E_{σ_4}, $E_{\sigma_4'}$, $E_{\sigma_4''}$ amd E_{ω_4} corresponding to the statistical weight parameters have been assigned[15] the values -0.2, 0.5, 0.9 and 0.6 kcal mol^{-1} in POM_4, respectively. For bond e2, the statistical weight matrix is:

$$U_{e2}=\begin{bmatrix}1 & \sigma & \sigma\\ 1 & \sigma & \sigma\omega\\ 1 & \sigma\omega & \sigma\end{bmatrix} \tag{12}$$

Here the energies $E_\sigma=0.5$ and $E_\omega=2.0$ kcal mol^{-1} have been assigned for a PM chain[8].

Since the chemical structure at carbon (*C) in *Figure 3b* is similar to that of one repeating unit of poly[oxy(1-alkylethylene)][14] the statistical weight matrix of b2 is taken directly from the result for bond b in ref. 14. It is given as follows:

$$U_{b2}=\begin{bmatrix}\gamma\omega'+\delta & 1+\gamma\omega'+\delta & 0\\ \gamma & 1+\gamma & 0\\ \gamma+\delta & \omega(1+\gamma+\delta) & 0\end{bmatrix} \tag{13}$$

where energies E_γ, $E_{\omega'}$ and E_δ associated with the statistical weight parameters are 0.5, 0.7 and 1.0 kcal mol^{-1}, respectively.

For bonds e2′ and e3′ in *Figure 3c*, the statistical weight matrices, with the aid of a model, may be derived as:

$$U_{e2'}=\begin{bmatrix}1 & \sigma & \sigma\\ 1 & \sigma\omega_4 & 0\\ \omega_4 & 0 & \sigma\end{bmatrix} \tag{14}$$

and

$$U_{e3'}=\begin{bmatrix}\sigma_2\sigma_2'\omega_2 & \sigma_2'\sigma_4 & \sigma_2'\beta\\ \sigma_2(1+\sigma_2'\omega_2) & \sigma_4(1+\sigma_2') & \beta\omega_4(1+\sigma_2')\\ \sigma_2(1+\sigma_2'\omega_2) & \sigma_4\omega_4(1+\sigma_2') & \beta(1+\sigma_2')\end{bmatrix} \tag{15}$$

Here energies corresponding to statistical weight parameters in these matrices are the same as those given in ref. 15. The other matrices are the same as those derived for *Figure 3a*.

SIMULATION PROCEDURE

The algorithm that is used here has been described in paper 1. In order to simulate triols, the algorithm was modified for three-arm star monomers. In brief, the central carbon atoms (*C) of POP triols (*Figure 1*) and diisocyanates are randomly distributed in a cubical box, whose edge length is determined by the total volume of its components. Once again, the arm lengths are generated out from the centre carbon atom (*C) by use of a Monte Carlo method based on the rotational isomeric state (RIS) theory. The statistical weight matrices needed for a Monte Carlo–RIS method have been described above. From this point on, the simulation procedure was the same as that used in the preceding paper.

In the simulations, 10000 POP triol molecules were generated with isotactic chains, since isotactic and atactic chains have the same distribution functions as shown in paper 1. The number of crosslinking agents, N_c is given by:

$$N_c=3r_rN_p/f_b \tag{16}$$

where r_s is the stoichiometric ratio of the crosslinker's functional units –NCO (B) to the number of functional units on the star molecules –OH (A), N_p is the number of star molecules and $f_b=2$ is the functionality of the crosslinking reagent. As before, the crosslinkers were treated as sticks. The length ($L=1.37$ nm) of 4,4′-diphenylmethane diisocyanate (MDI) was determined from the groups (methylene, phenyl and isocyanate) and the bond angle ($\theta=112°$)[9] at the methylene carbon. Simulations were done for two different POP triols (Niax triol LHT-240 and Niax triol LG-56)[9] in the bulk at 60°C with the stoichiometric ratios r_s shown in *Table 2*. To simulate the solution studies, calculations were performed for LHT-240[10] at 25°C with the stoichiometric ratios, r_s shown in *Table 3*. The number-average molecular weights[9] are 708 for LHT-240 and 2630 for LG-56. The number-average functionalities[9] f_n are 2.89 (LHT-240) and 2.78 (LG-56). The densities[16] of triols used in these simulations are 1.022 g cm^{-3} for LHT-240 and 1.066 g cm^{-3} for LG-56, and the density[17] of MDI is 1.19 g cm^{-3}. The calculation of $\langle r^2\rangle_0$ was previously described in equation (7) of paper 1. The values of $2\langle r^2\rangle_0^{1/2}$ used to suppress gel–gel reactions are 2.86 nm

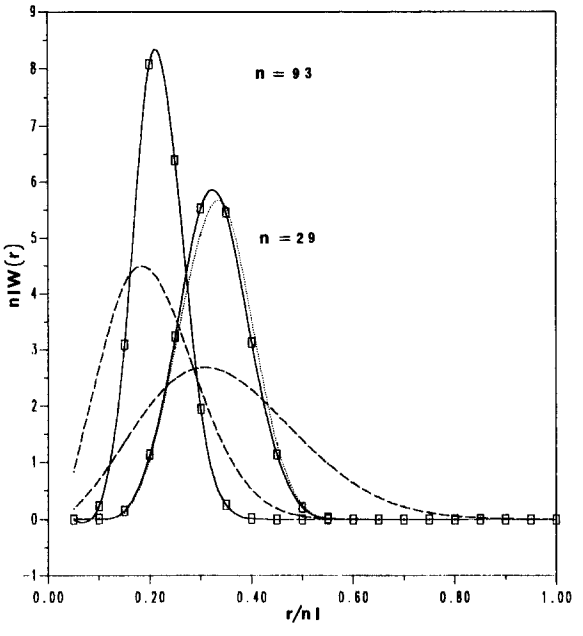

Figure 4 End-to-end distance distribution functions obtained from the Monte Carlo–RIS scheme for POP triols having $n=29$ and 93 at 60°C (full curves) and at 25°C (dotted curve). The distributions for $n=29$ and 93 are also shown (broken curves)

for LHT-240 and 6.12 nm for LG-56. All results obtained are averages over at least four configurations for each set of parameters.

RESULTS AND DISCUSSION

Distribution functions

The distances r between pairs of two –OH groups were calculated with use of the matrices prescribed above for the models shown in *Figures 2* and *3*. The end-to-end distances r were normalized by nl and were grouped into 20 intervals to obtain the non-Gaussian distribution $W(r)$. The procedures is the same as that in paper 1.

Results at 60°C obtained for the star polyols having 29 (LHT-240) and 93 (LG-56) skeletal bonds are shown in *Figure 4* as full curves. The dotted curve shows the distribution function for LHT-240 at 25°C. The broken curves in *Figure 4* show the results of Gaussian distributions, which were calculated from equation (6) of paper 1 by using the characteristic ratios[18] $C_n=4.20$ for $n=29$ and 4.77 for $n=93$. It can be seen that the distribution functions are similar to those given in the preceding paper.

Gel and sol generated by simulations

The weight fractions w_x of selected molecules (x-mers) in the sol for $M_n=708$ (LHT-240) and 2630 (LG-56) are listed in *Table 1*. *Table 1* only presents the results obtained from the first two systems for each molecular weight ($r_s=0.990$ and 0.893 for $M_n=708$ and $r_s=0.979$ and 0.891 for $M_n=2630$). Other systems follow the same trends, and have been omitted to conserve space. For low sol fractions there are two dominant types of molecules in the sol: these are star monomers and cyclic molecules that contain two-arm loop monomers, double-edge loops and dumbbells. It can be seen that two-arm loop monomers and dumbbells are found in substantial concentrations with $r_s\sim 1.0$. These two types of molecules constitute ~71% of the weight of the sol for $M_n=708$ and ~54% for $M_n=2630$. However, since –OH groups are predominant for $r_s\sim 0.89$, the star monomers are the most abundant molecules for this case.

In order to facilitate comparisons of the results of computer simulations with those of experiment and theoretical calculations, simulations were performed by adjusting the capture radius to give the same sol fraction w_s as those obtained experimentally[9,10]. Data in columns 3 and 4 of *Tables 2* and *3* are the weight fractions of the sol obtained in the experiments and from simulations, respectively. For the systems of $r_s\sim 1.0$ (bulk and solutions), the experimental weight fractions of the sol are very low, and the sol fractions from simulations are greater than those of the experiments. This is because the weight fractions w_x of both two-arm loop monomers and dumbbells are very high (see *Table 1*). The dumbbells are inert and some two-arm loop monomers are inert too, since 22% of LG-56 and 11% of LHT-240 are diols, not triols.

The number fraction of active groups, which is defined as the ratio of the number of active groups in the gel to the total number of monomer arms incorporated into the gel, are entered in column 7 of *Tables 2* and *3*. The active groups are either –NCO groups or free –OH groups. From the results of these simulations, there are ~4% of free NCO groups for the systems with $r_s\sim 1$. According to the experimental work of Stepto[19,20], side-reactions that form allophanate groups are possible. It is likely that the urethane groups on the sol molecules were reacted with the free –NCO groups in the gel. Therefore, allophanate linkages are probably the cause of the lower experimental sol fractions.

Values entered into columns 5 and 6 of *Tables 2* and *3* are the extents of reaction of NCO groups calculated from the weight fractions of sol by use of cascade theory[9,10] and from these simulations, respectively. The differences between the extents of reaction from theoretical calculations and from simulations are about 2–4%, which may be attributed to the fact that in cascade theory only intermolecular conversions of –NCO groups[12] are permitted, except for loop formation, and to the fact that the simulations omit side-reactions.

The last column of *Tables 2* and *3* shows the fraction of loops s, which is the fraction of bonds wasted in elastically inactive loops. The fraction of loops is given by the theory of Dušek and Vojta[12] as:

$$s=\sigma/(a+\sigma) \tag{17}$$

where σ and a are the number of intra- and intermolecular reactions, respectively. The theoretical calculation of σ is dependent on the factor[13]:

$$\Lambda=(3/2\pi QL^2)^{3/2}/N_A \tag{18}$$

Table 1 The dominant sol constituents[a]

x-mer	Graph	10^2w_x[b]	10^2w_x[c]	10^2w_x[d]	10^2w_x[e]
1		0.05	0.45	0.36	1.37
		0.32	0.31	0.77	0.92
2		0.01	0.05	0.06	0.08
		0.20	0.15	0.20	0.16
Others		0.19	0.75	0.40	2.61

[a] Simulations performed in the bulk
[b] $M_n=708$, $r_s=0.990$, $p=0.958$ and $w_s=0.77\%$
[c] $M_n=708$, $r_s=0.893$, $p=0.987$ and $w_s=1.71\%$
[d] $M_n=2630$, $r_s=0.979$, $p=0.963$ and $w_s=1.79\%$
[e] $M_n=2630$, $r_s=0.891$, $p=0.984$ and $w_s=5.14\%$

Table 2 The extent of reaction of NCO groups and fraction of loops[a]

M_n	r_s[b]	w_s[c]	w_s[d]	p[e]	p[f]	a_c[g]	s[h]
708	0.990	0.004	0.008	0.983	0.958	0.084	0.078
(LHT-240)	0.893	0.013	0.017	0.964	0.987	0.110	0.074
	0.813	0.039	0.039	0.970	0.988	0.179	0.072
	0.746	0.097	0.098	0.970	0.998	0.203	0.064
	0.694	0.168	0.168	0.976	1.000	0.221	0.057
	0.645	0.296	0.296	0.979	1.000	0.236	0.049
	0.621	0.362	0.362	0.984	1.000	0.239	0.051
2630	0.979	0.015	0.018	0.936	0.963	0.074	0.050
(LG-56)	0.891	0.051	0.051	0.937	0.984	0.108	0.047
	0.814	0.170	0.170	0.923	0.965	0.143	0.037
	0.723	0.318	0.351	0.943	0.973	0.182	0.032
	0.689	0.397	0.395	0.951	0.974	0.197	0.030
	0.653	0.577	0.576	0.952	0.960	0.208	0.026
	0.630	0.651	0.650	0.960	0.952	0.212	0.024

[a] LG-56 and LHT-240, simulation carried out in the bulk
[b] r_s=[NCO]/[OH]
[c] The weight fraction of the sol, ref. 9
[d] The weight fraction of the sol, this work
[e] The extent of reaction of NCO groups, ref. 9
[f] The extent of reaction of NCO groups, this work
[g] The number fraction of active groups in the gel
[h] The fraction of loops=intramolecular reaction/total reactions in the gel

Table 3 The extent of reaction of NCO groups and fraction of loops[a]

r_s[b]	v^0[c]	w_s[d]	w_s[e]	p[f]	p[g]	a_c[h]	s[i]
1.000	0.8	0.0015	0.0075	0.981	0.952	0.083	0.086
	0.6	0.0031	0.0145	0.975	0.953	0.082	0.117
	0.5	0.0041	0.0160	0.975	0.954	0.084	0.123
0.769	0.8	0.0842	0.0875	0.967	0.990	0.168	0.075
	0.6	0.0952	0.0950	0.969	0.990	0.168	0.086
	0.5	0.1040	0.1050	0.970	0.990	0.165	0.098
0.667	0.8	0.2490	0.2480	0.978	1.000	0.209	0.062
	0.6	0.2605	0.2610	0.982	1.000	0.204	0.073
	0.5	0.2675	0.2660	0.986	1.000	0.203	0.080

[a] LHT-240, simulations carried out in various solutions
[b] r_s=[NCO]/[OH]
[c] $v^0=1-v_d^0$, v_d^0=the volume fraction of solvent
[d] The weight fraction of the sol, ref. 10
[e] The weight fraction of the sol, this work
[f] The extent of reaction of NCO groups, ref. 10
[g] The extent of reaction of NCO groups, this work
[h] The number fraction of active groups in the gel
[i] This work, the fraction of loops

which was derived from the Gaussian distribution function. Here N_A is Avogadro's number, Q is the number of main-chain atoms in a statistical segment, and L is the length per main-chain atom. The fraction of loops has been calculated by Ilavský and Dušek[9,10]; they find values of s of about 2–3% for the systems cured in the bulk and 2–4% for the systems in various solutions. The theoretical calculations also show that systems with higher stoichiometric ratios give higher values for the fraction of loops. Values obtained from simulations are always higher than those calculated by theory. Values in the last column of *Table 2* are 2.4–7.8% for the systems simulated in the bulk and those in the last column of *Table 3* are 6.2–12.3% for the systems simulated in various solutions. Both simulations and theory[9,10] give the same trend, i.e. higher values for the stoichiometric ratios give more loops.

Defect structures in the gel

There are two major types of structural irregularities that exist in the networks. These are two-arm dangling loops and two-arm dangling ends. Two-arm dangling loops arise when two active arms of a star molecule (monomer) connect to the same crosslinker. Two-arm dangling ends are formed when only one arm of a star molecule is incorporated into the network. The population η of network imperfections is defined as the number of fragments of a particular type that occur per star monomer incorporated in the gel.

The systems that were simulated are presented in *Tables 2* and *3*. For clarity, only some of these systems are shown in the figures. *Figures 5* and *6* show the various populations for two-arm dangling ends as a function of the extent of reaction of NCO groups. The symbols in these figures have been used in previous studies[21], namely

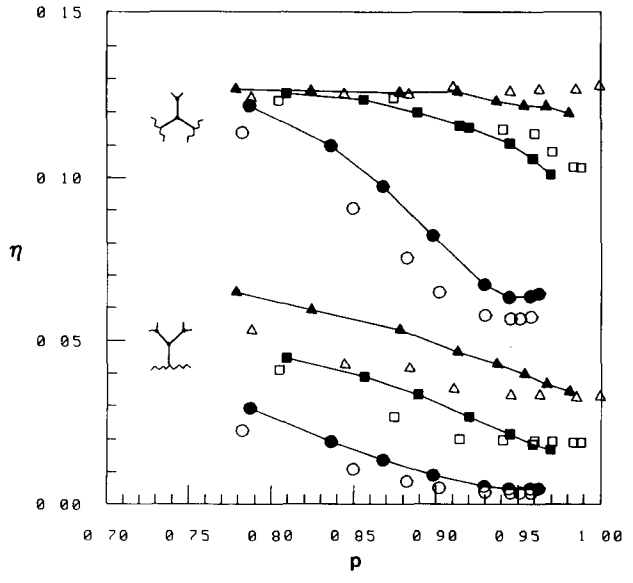

Figure 5 Plots of (from top) populations of 'I' and 'V' dangling ends vs. the extent of reaction for different molecular weights and for various stoichiometric ratios. LG-56: $r_s=0.979$ (●), 0.814 (■) and 0.689 (▲): $r_s=0.990$ (○), 0.813 (□) and 0.694 (△)

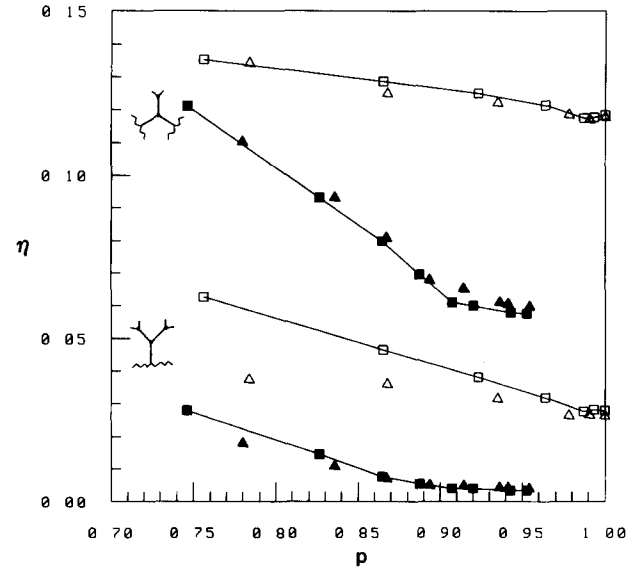

Figure 6 Plots of (from top) populations of 'I' and 'V' dangling ends vs. the extent of reaction for LHT-240, for various stoichiometric ratios, and for various dilutions. $r_s=1.0$: $v^0=0.8$ (■) and 0.5 (▲). $r_s=0.667$: $v^0=0.8$ (□) and 0.5 (△)

'I' and 'V'. The dot on the symbols represents the centre carbon (*C) of a star monomer, and the remainder of the network is indicated by jagged lines. It can be seen that, at high conversion, these two types of dangling ends, I and V, are insensitive to the two different molecular weights (*Figure 5*). *Figure 6* shows that the populations of I and V types are independent of dilution but are dependent on stoichiometric ratios. For the systems with $r_s \sim 1.0$ in *Figures 5* and *6*, type V approaches zero at high conversion of NCO groups and, unlike the previous studies[21,22], type I fragments remain near 6% owing to the suppression of gel–gel reactions. *Figures 5* and *6* also show that the smaller the stoichiometric ratio r_s, the greater is the population of dangling ends. This is due to the fact that, when OH groups are predominant, networks have more dangling ends. From *Figures 5* and *6*, it is found that the population of I type fragments increases by about 6% and the population of V type increases by $\sim 3\%$ as r_s varies from ~ 1.0 to ~ 0.7.

Variations in the population of two-arm dangling loops with the extent of reaction of NCO groups are shown in *Figures 7* and *8*. Symbols used are similar to those above. *Figure 7* shows that the population of loops for systems cured in the bulk depends on both molecular weight and r_s. It can be seen that the population of loops increases for lower molecular weight or for higher r_s. For example, the lowest population of loops is found for $M_n=2630$ and $r_s=0.689$ (see *Figure 7*, the lowest full curve). *Figure 8* shows that, at various dilutions v^0, more loops are formed at high dilution, or at higher r_s. The results shown in *Figures 7* and *8* are similar to those of the previous studies[21,22] for telechelic polymers.

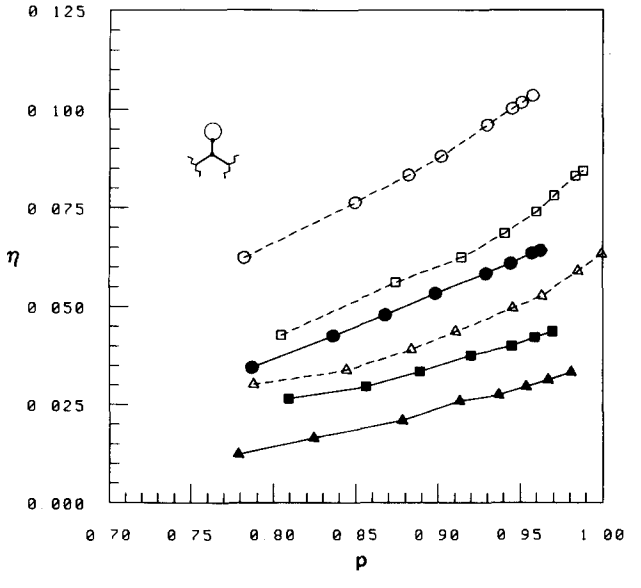

Figure 7 Population of dangling loops: symbols are the same as those of *Figure 5*

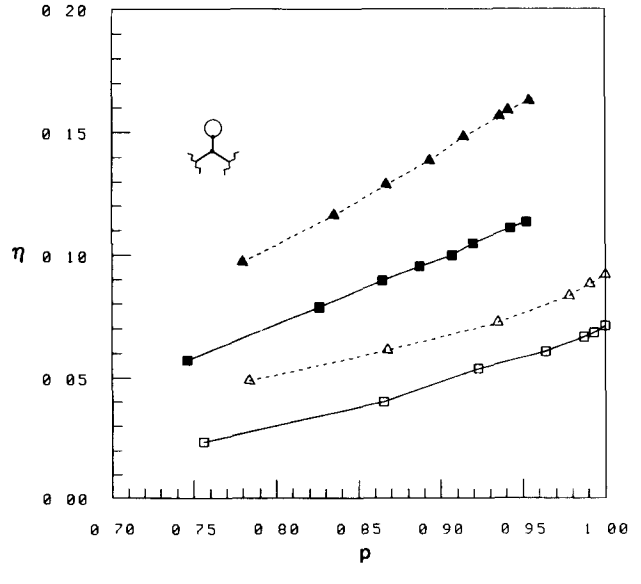

Figure 8 Population of dangling loops: symbols are the same as those of *Figure 6*

Table 4 The concentration of elastically active network chains and experimental reduced modulus[a]

M_n	r_s[b]	deg 2[c]	$10^4 v_{eg}$[d]	$10^4 v_{e1}$[e]	$10^4 G_{r1}$[f]	$10^4 \xi_{e1}$[g]
708	0.990	0.227	12.33	6.486	8.529	2.162
(LHT-240)	0.893	0.257	7.077	5.603	6.193	1.868
	0.813	0.338	4.696	2.951	4.183	0.984
	0.746	0.361	2.737	2.261	3.002	0.754
	0.694	0.377	1.684	1.655	1.230	0.552
	0.645	0.396	0.825	1.268	0.521	0.423
	0.621	0.400	0.575	1.013	0.339	0.338
2630	0.979	0.287	2.180	2.251	3.791	0.750
(LG-56)	0.891	0.335	1.320	1.826	2.359	0.609
	0.814	0.402	0.543	1.231	1.254	0.410
	0.723	0.439	0.241	0.756	0.640	0.252
	0.689	0.442	0.158	0.580	0.310	0.193
	0.653	0.461	0.057	0.333	0.118	0.111
	0.630	0.468	0.035	0.242	0.080	0.081

[a] LG-56 and LHT-240, reactions carried out in the bulk
[b] r_s = [NCO]/[OH]
[c] The number fraction of unsaturated monomers, degree = 2
[d] Theoretical concentration (mol cm^{-3}) of elastically active network chains, ref. 9
[e] Concentration (mol cm^{-3}) of elastically active network chains, this work
[f] Experimental reduced modulus (mol cm^{-3}), ref. 9
[g] Concentration (mol cm^{-3}) of cycle rank, this work

Theories of rubber elasticity

There are two famous models for rubber elasticity—affine and phantom. If the fluctuations of the network are fully suppressed, the displacements of the network junctions are affine with respect to macroscopic strain. According to the affine model, the equilibrium modulus can be represented as[23,24]:

$$E_G^a = RTv_e v_2^{1/3}(V_{gel}/V_f)^{2/3} \quad (19)$$

where V_{gel} is the volume of the dry, unstrained network and $v_e = v_a/V_{gel}$ is the number of elastically active chains per unit volume of dry network. Here v_2 is the volume fraction of the network in the swollen state and $V_f = V_{gel} + V_{sol} + V_{dil}$ is the volume of the system at the time of network formation. (V_{sol} and V_{dil} are the volume of the sol and diluent, respectively.) If the networks are prepared in the bulk and the modulus measurements are carried out on the dry unextracted elastomer, $V_f = V_{gel} + V_{sol}$ and $v_2 = V_{gel}/(V_{gel} + V_{sol})$. In this case, equation (19) becomes:

$$E_G^a = RTv_{e1}w_g \quad (20)$$

where $w_g = V_{gel}/(V_{gel} + V_{sol})$ is the weight fraction of the gel (assuming the densities of gel and sol are the same). To aid comparisons, equation (20) may be expressed by a reduced form:

$$G_{r1}^a = v_{e1} = E_{G1}^a/w_g RT \quad (21)$$

If the network reactions are carried out by various solutions, and the modulus measurements are performed on the samples after complete polymerization (samples containing solvent), $V_f = V_{gel} + V_{sol} + V_{dil}$ and $v_2 = V_{gel}/V_f = v^0 w_g$, where v^0 is the volume fraction of the polymer (including both gel and sol) at the end of network formation, i.e. $v^0 = 1 - v_d^0$, where v_d^0 is the volume fraction of the solvent during network formation. Equation (19) can then be expressed as:

$$E_{G2}^a = RTv_{e2}w_g v^0 \quad (22)$$

and in reduced form as:

$$G_{r2}^a = v_{e2} = E_{G2}^a/w_g v^0 RT \quad (23)$$

For the phantom model, it is assumed that the fluctuations of junctions are independent of deformation, and there are no constraints on the junctions. Flory[25] has developed the relationship between the elastic free energy and cycle rank for a Gaussian network. If the stress–strain measurements are carried out in the swollen state, the equilibrium modulus for this model is:

$$E_G^a = RT\xi_e v_2^{1/3}(V_{gel}/V_f)^{2/3} \quad (24)$$

where $\xi_e = \xi_a/V_{gel}$ is the cycle rank per unit volume. The reduced moduli corresponding to the derived conditions of equations (20) and (22) for the phantom networks are:

$$G_{r1}^{ph} = \xi_{e1} = E_{G1}^{ph}/w_g RT \quad (25)$$

and

$$G_{r2}^{ph} = \xi_{e2} = E_{G2}^{ph}/w_g v^0 RT \quad (26)$$

for the network prepared in the bulk and solutions, respectively. In order to compare the results of simulations with those of Ilavský and Dušek[9,10], the Scanlan–Case[26,27] definitions have been adopted, i.e. an active junction is joined by at least three paths to the network, and an active chain is connected at both of its ends to active junctions. In these simulations, an active junction is a vertex (original star monomer) of a graph whose degree is equal to 3, and an active chain is attached to two different active junctions, i.e. two arms from different monomers are connected to the same crosslinker. A junction (of degree = 3) attached to a two-arm dangling end or a two-arm dangling loop is excluded from the count of active junctions. Using this counting procedure, active chains ν_a and active junctions μ_a can be readily obtained from the results of the simulations. The cycle rank ξ_a can then be deduced from the equation:

$$\xi_a = \nu_a - \mu_a \quad (27)$$

Tables 4 and *5* list the simulation results for the concentrations of active chains (column 5) and cycle ranks (the last column). Theoretical calculations of the concentrations of active chains (column 4) based on

Table 5 The concentration of elastically active network chains and experimental reduced modulus[a]

r_s[b]	v^0[c]	deg 2[d]	$10^4\nu_{eg}$[e]	$10^4\nu_{e2}$[f]	10^4G_{r2}[g]	$10^4\xi_{e2}$[h]
1.000	0.8	0.229	11.05	6.099	8.990	2.033
	0.6	0.224	9.92	4.906	7.621	1.647
	0.5	0.222	9.47	4.597	7.364	1.533
0.769	0.8	0.321	3.00	3.098	2.979	1.033
	0.6	0.318	2.77	2.763	2.430	0.921
	0.5	0.316	2.58	2.380	1.900	0.974
0.667	0.8	0.379	1.09	1.730	0.639	0.577
	0.6	0.361	0.99	1.566	0.594	0.520
	0.5	0.367	0.96	1.311	0.460	0.437

[a] LHT-240, reactions carried out in various solutions
[b] r_s=[NCO]/[OH]
[c] $v^0=1-v_d^0$, v_d^0=the volume fraction of solvent
[d] The number fraction of unsaturated monomers, degree=2
[e] The theoretical concentration (mol cm^{-3}) of elastically active network chains, ref. 10
[f] Concentration (mol cm^{-3}) of elastically active network chains, this work
[g] Concentration (mol cm^{-3}) of cycle rank, this work
[h] Experimental reduced modulus (mol cm^{-3}), ref. 10

cascade theory[12] and experimental reduced moduli (column 6) are also listed in *Tables 4* and *5* for comparison. Column 3 of *Tables 4* and *5* shows the number of unsaturated monomers per monomer incorporated into the gel. Here each of the unsaturated monomers, which is an inactive junction, has degree 2. Remember that the percentage of diols is 22% for LG-56 and 11% for LHT-240; hence the values of the fractions of unsaturated monomer are very high (see column 3 of *Tables 4* and *5*). Computer simulations show, for example, that ~50% of the monomers incorporated into the gel is counted as inactive junctions for the LG-56 system with $r_s=0.979$ for reactions carried out in the bulk (see *Figures 5* and *7* and *Table 4*).

For LHT-240 in *Table 4*, the concentrations of active chains obtained from the simulations for the first three systems are lower than those from theoretical calculations. This is because the simulations give more loops and unsaturated monomers than does the theory. The agreement is very good for the fourth and fifth systems. Simulations give higher values than theoretical calculations for the last two systems. Similarly, the agreement is remarkably good between the simulations and the theoretical calculations for the first two LG-56 systems in *Table 4*, but simulations give higher values for the systems with $r_s=0.814$ to 0.630. In *Table 5*, theoretical calculations give higher values than do simulations for the systems at $r_s=1.0$, there is good agreement for the systems at $r_s=0.769$, and theoretical calculations underestimate the concentrations of active chains for the systems at $r_s=0.667$.

The experimental reduced moduli have been given by[9,10]:

$$G_{r1}=G_1/w_gRT \tag{28}$$

and

$$G_{r2}=G_2/w_gv^0RT \tag{29}$$

where G_1 and G_2 are the experimental equilibrium moduli measured on dry unextracted samples[9] and on samples after complete polymerization (containing solvent)[10]. Equations (28) and (29) are similar to equations (21) and (23) or to equations (25) and (26). Results from simulations for concentrations of active chains and cycle ranks can be used to compare with the experimental moduli, thereby determining whether the experimental systems are best described by the affine or the phantom model.

From *Tables 4* and *5*, it can be seen that, for larger values of r_s (the first three systems of LHT-240 in *Tables 4* and *5* and first two systems of LG-56 in *Table 4*), the values of the experimental moduli (column 6) are much larger than those given by cycle ranks evaluated from the simulations (column 7). For other systems studied here, the elastic behaviour of the real networks lies between the phantom and affine limits. Previous studies[1,22] have shown that networks prepared with low-molecular-weight polymers seem to have phantom chain behaviour. It was also shown[22] that networks seem to have affine chain behaviour when prepared with high-molecular-weight polymer in the bulk or at high concentration. The large values of the experimental moduli for the present MDI-based systems may be attributed to segmentation effects. The aggregation of hard segments (OH–MDI) through hydrogen bonding[28–31] C=O·····H—N between the N–H group and the urethane carbonyl group of adjacent segments has been found in polyurethane elastomers. The high values of the experimental moduli seem to implicate network reinforcement through hydrogen bonding.

Segmentation effects in MDI urethane networks are well known[28–31]. Professor R. F. T. Stepto (private communication) has also come to the conclusion that the MDI networks of this study have enhanced moduli owing to segmentation effects. Hydrogen bonding is probably not the only cause of this aggregation. Large π–π interactions between the phenylene groups of MDI molecules are also likely to be of considerable importance in the formation of MDI clusters. We did not take clustering into effect in this study but instead suggest that the algorithm here could be modified without difficulty to model clustered crosslinkers right from the beginning. In effect one would have a molecule of larger volume with higher functionality that would take the place of the monomeric difunctional MDI units we used. Such simulations should give the average number of MDI molecules involved in a cluster. Further investigation of this effect will be the subject of a future publication.

In *Table 4*, LHT-240 systems with $r_s=0.746$ and 0.694 and the LG-56 systems with $r_s=0.814$ and 0.723 show affine chain behaviour, because the experimental moduli of these systems are about a factor of 3 larger than values from simulations (the last column). As seen in *Table 5*, it is clear that networks seem to have affine chain behaviour when prepared in solution with $r_s=0.769$.

For the last two LHT-240 and LG-56 systems in *Table 4* and the last three systems in *Table 5*, very good agreement between experimental moduli and the results of simulations is found. Since these systems have high populations of dangling ends (see *Figures 5* and *6*) they have loose network structures, and hence may be subject to fewer constraints on their junctions. This interpretation according to the Flory–Erman theory[32–35] provides a consistent description of the results, but might not be the only explanation.

ACKNOWLEDGEMENTS

The authors are grateful for support from the Department

of Energy, Grant DE-FG06-84ER45123. We also thank Professor K. Dušek for making his data available to use. This work is a contribution to an IUPAC-sponsored programme on the structure of polymer networks.

REFERENCES

1 Lee, K.-J. and Eichinger, B. E. *Polymer* 1989, **31**, 406
2 Hill, J. L. and Stepto, R. F. T. *Trans. Faraday Soc.* 1971, **67**, 3202
3 Yoon, D. Y. and Flory, P. J. *J. Chem. Phys.* 1974, **61**, 5366
4 Flory, P. J. and Chang, V. W. C. *Macromolecules* 1976, **9**, 33
5 Mark, J. E. and Curro, J. G. *J. Chem. Phys.* 1983, **79**, 5705
6 Mark, J. E., DeBolt, L. C. and Curro, J. G. *Macromolecules* 1986, **19**, 491
7 DeBolt, L. C. and Mark, J. E. *Macromolecules* 1987, **20**, 2369
8 Flory, P. J. 'Statistical Mechanics of Chain Molecules', Interscience, New York, 1969
9 Ilavský, M. and Dušek, K. *Polymer* 1983, **24**, 981
10 Ilavský, M. and Dušek, K. *Macromolecules* 1986, **19**, 2139
11 Ilavský, M. and Dušek, K. *Polym. Bull. (Berlin)* 1982, **8**, 359
12 Dušek, K. and Vojta, V. *Br. Polym. J.* 1977, **9**, 164
13 Dušek, K., Gordon, M. and Ross-Murphy, S. B. *Macromolecules* 1978, **11**, 236
14 Abe, A., Hirano, T., Tsuji, K. and Tsuruta, T. *Macromolecules* 1979, **12**, 1100
15 Abe, A. and Mark, J. E. *J. Am. Chem. Soc.* 1976, **98**, 6468
16 Kastens, A. S. 'High Polymers' (Ed. N. G. Gaylord), Interscience, New York, 1963, Vol. 13, Part 1, p. 228
17 Saunders, J. H. and Frisch, K. C. 'High Polymers', Interscience, New York, 1962, Vol. 16, Part 1, p. 348
18 Abe, A., private communication
19 Stanford, J. L. and Stepto, R. F. T. *Br. Polym. J.* 1977, **9**, 124
20 Stepto, R. F. T. and Waywell, D. R. *Makromol. Chem.* 1972, **152**, 263
21 Leung, Y. K. and Eichinger, B. E. *J. Chem. Phys.* 1984, **80**, 3877, 3885
22 Lee, K.-J. and Eichinger, B. E. *Macromolecules* in press
23 Flory, P. J. 'Principles of Polymer Chemistry', Cornell University Press, Ithaca, NY, 1953
24 Treloar, L. R. G. 'The Physics of Rubber Elasticity', Clarendon, Oxford, 1975
25 Flory, P. J. *Proc. R. Soc. Lond.* (*A*) 1976, **351**, 351
26 Scanlan, J. *J. Chem. Phys.* 1960, **43**, 501
27 Case, L. C. *J. Polym. Sci.* 1960, **45**, 397
28 Blackwell, J. and Gardner, K. H. *Polymer* 1979, **20**, 13
29 Seymour, R. W., Allegrezza. A. E. Jr and Cooper, S. L. *Macromolecules* 1973, **6**, 896
30 Seymour, R. W. and Cooper, S. L. *Macromolecules* 1973, **6**, 48
31 Srichatrapimuk, V. W. and Cooper, S. L. *J. Macromol. Sci., Phys.* (*B*) 1978, **15**, 267
32 Flory, P. J. *J. Chem. Phys.* 1977, **66**, 5720
33 Erman, B. and Flory, P. J. *J. Chem. Phys.* 1978, **68**, 5363
34 Flory, P. J. and Erman, B. *Macromolecules* 1982, **15**, 800
35 Erman, B. and Flory, P. J. *Macromolecules* 1982, **15**, 806